Accelerated Publications

Structure of the Mammalian CoA Transferase from Pig Heart†

Katherine S. Bateman,‡ Edward R. Brownie,§ William T. Wolodko,§ and Marie E. Fraser*,‡,||

Department of Biochemistry, University of Western Ontario, London, Ontario, Canada, N6A 5C1, and Department of Biochemistry, University of Alberta, Edmonton, Alberta, Canada, T6G 2H7

Received September 4, 2002; Revised Manuscript Received October 25, 2002

ABSTRACT: Ketoacidosis affects patients who are deficient in the enzyme activity of succinyl-CoA:3-ketoacid CoA transferase (SCOT), since SCOT catalyses the activation of acetoacetate in the metabolism of ketone bodies. Thus far, structure/function analysis of the mammalian enzyme has been predicted based on the three-dimensional structure of a CoA transferase determined from an anaerobic bacterium that utilizes its enzyme for glutamate fermentation. To better interpret clinical data, we have determined the structure of a mammalian CoA transferase from pig heart by X-ray crystallography to 2.5 Å resolution. Instrumental to the structure determination were selenomethionine substitution and the use of argon during purification and crystallization. Although pig heart SCOT adopts an α/β protein fold, resembling the overall fold of the bacterial CoA transferase, several loops near the active site of pig heart SCOT follow different paths than the corresponding loops in the bacterial enzyme, accounting for differences in substrate specificities. Two missense mutations found associated with SCOT of ketoacidosis patients were mapped to a location in the structure that might disrupt the stabilization of the amino-terminal strand and thereby interfere with the proper folding of the protein into a functional enzyme.

Succinyl-CoA:3-ketoacid CoA transferase (SCOT, EC 2.8.3.5)[1] is a mitochondrial enzyme in mammals that is essential for the metabolism of ketone bodies. SCOT is responsible for the transfer of coenzyme A (CoA) from succinyl-CoA to acetoacetate. Once activated, acetoacetyl-CoA is further metabolized into acetyl-CoA which can either enter the citric acid cycle or be stored ultimately as a fatty acid. Patients who are deficient in SCOT activity suffer from episodic ketoacidosis, usually during periods of fasting or illness. Moreover, it is suspected that SCOT deficiency is underdiagnosed (*1, 2*).

Early studies of SCOT from pig heart, sheep kidney, or rat brain showed that the mammalian enzyme exists as a homodimer, with two active sites (*3*−*7*). The transfer of CoA from one substrate to another is via a ping-pong mechanism, involving the formation of a covalent thiolester bond between coenzyme A and a glutamate residue at each active site of the enzyme (Scheme 1) (*8*). During purification, especially in the absence of proteinase inhibitors, the monomer can be nicked without disrupting the structure, and the enzyme is fully active (*6, 9*−*11*). Cloning and DNA sequencing of the pig heart enzyme showed that the mature monomer (without the signal peptide for transit into mitochondria) is a polypeptide of 481 amino acid residues, with a molecular weight of 51 197 (*10*). The stretch of polypeptide where the nicking takes place was proposed to adopt a helix−turn−helix conformation, connecting amino- and carboxy-terminal fragments that had molecular weights of 2.8×10^4 and 2.4×10^4, respectively (*10*). The monomer can also undergo autolytic fragmentation if first treated with succinyl-CoA or acetoacetyl-CoA (*12*). The glutamate−CoA thiolester is thought to react with the amide nitrogen atom of the glutamate residue, resulting in cleavage of the peptide bond, release of the CoA molecule, and formation of pyroglutamate. The nicking and autolytic fragmentation were used to identify the active-site glutamate residue as Glu 305, by peptide sequencing (*13*) and by determining the mass of the peptide by mass spectrometry (*11*).

† This work was funded by an operating grant from the Canadian Institutes of Health Research (MOP-42446). Crystallization and computational resources were purchased with awards from the Academic Development Fund, University of Western Ontario (Project 00-152), the Canada Foundation for Innovation (Project 3185), and an Equipment Grant from the Natural Sciences and Engineering Research Council of Canada (NSERC). M.E.F. was supported by an NSERC University Faculty Award. The crystallographic data were collected at beamline X26c NSLS/BNL through the NIH/RR Biology Mail-In Data Collection Program with beam time kindly provided by Annie Heroux.

* To whom correspondence should be addressed. Tel: 403-220-6145; 403-220-2773. Fax: 403-289-9311. E-mail: frasm@ucalgary.ca.

‡ University of Western Ontario.

§ University of Alberta.

|| Current address: Department of Biological Sciences, University of Calgary, 2500 University Drive NW, Calgary, AB, Canada, T2N 1N4.

[1] Abbreviations: CoA, coenzyme A; SCOT, succinyl-CoA:3-ketoacid CoA transferase; MAD, multiwavelength anomalous dispersion; GCT, glutaconate CoA transferase from *A. fermentans*; LB, Luria-Bertani; IPTG, isopropyl-β-D-thiogalactoside; OD_{600}, optical density at 600 nm; EDTA, ethylenediaminetetraacetic acid; P2000, poly(ethylene glycol); TrisCl, tris(hydroxymethyl)aminomethane hydrochloride; CNS, Crystallography and NMR System; F_o, observed structure factor amplitude; F_c, structure factor amplitude calculated from the model; s, standard deviation.

10.1021/bi020568f CCC: $22.00
Published on Web 11/14/2002

Scheme 1: Chemical Steps Likely Involved in the Ping-Pong Mechanism of Succinyl-CoA:3-Ketoacid CoA Transferase (*38*)

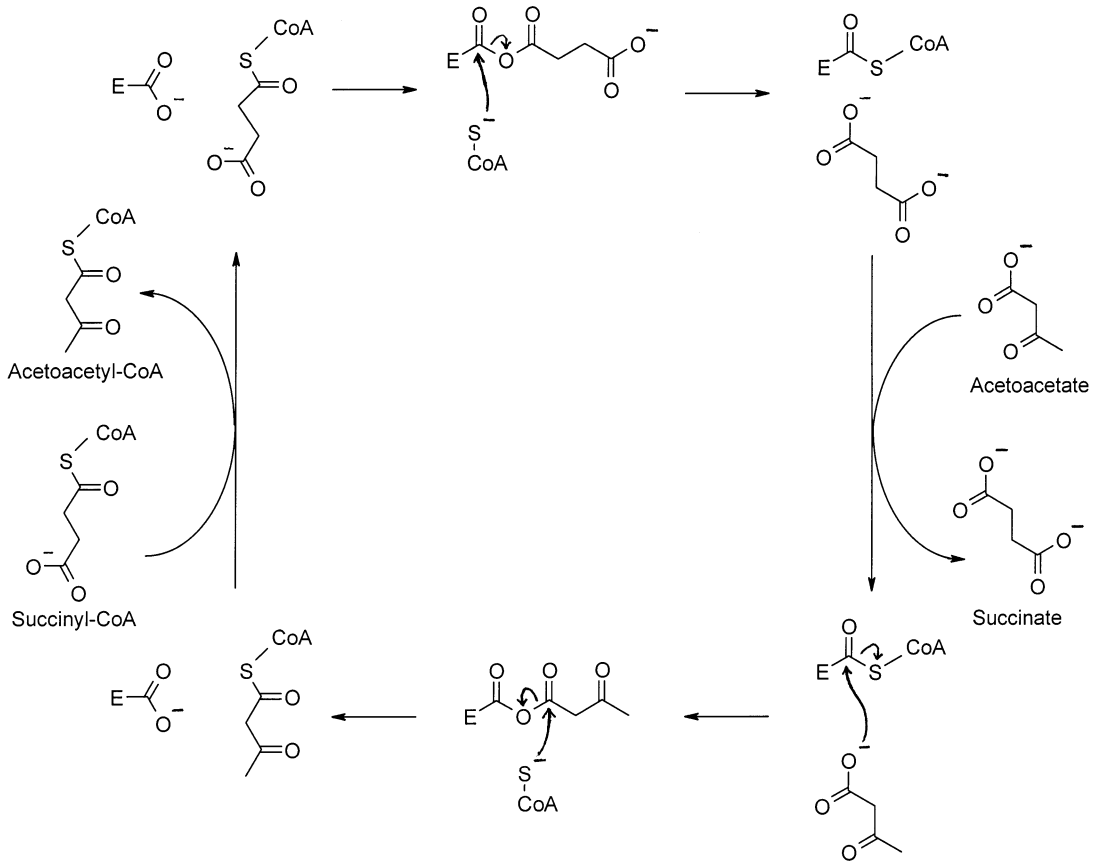

More recently, a homotetrameric form of pig heart SCOT was detected during purification of overexpressed enzyme for crystallization trials (*14*). The homotetramer was also shown to exist in preparations of SCOT purified from pig heart tissue, prior to the purification steps that use high concentrations of potassium chloride. In the presence of high concentrations of potassium chloride, the homotetramer dissociates to homodimers, and the use of common protocols involving potassium chloride may be why the presence of a homotetramer was not detected earlier. The physiological relevance of the homotetramer is not yet known, but the homotetramer is catalytically indistinguishable from the homodimer (*14*).

Another twist on our understanding of the role of the quaternary structure of pig heart SCOT has been presented by the group of Shoolingen−Jordan (*15*). Their work showed that although the enzyme is a homodimer with two active sites, apparently only one supports catalysis.

The structure of a CoA transferase from a bacterial source has been determined by X-ray crystallography (*16*). Glutaconate CoA transferase from *A. fermentans* (GCT) plays a role in the glutamate fermentation pathway in this anaerobic bacterium. The enzyme is a heterooctamer, made up of four copies of each of two different subunits, designated A and B. Structural similarity was observed between the A and B subunits, and a consensus matrix based on the structural alignment allowed the authors to construct sequence alignments with CoA transferases from different sources (*16*). It was predicted that these CoA transferases, including pig heart SCOT, would adopt the same fold, despite often very little sequence similarity. The amino-terminal fragment of SCOT more closely corresponds to the A subunit of GCT, while the carboxy-terminal fragment of SCOT more closely corresponds to the B subunit. The active site glutamate residue Glu 305 of SCOT aligns with Glu B54 of GCT. On the basis of the GCT structure, Fukao et al. built a homology model of human SCOT in order to examine several missense mutations associated with the enzyme from patients suffering ketoacidosis (*17*). The sequence identity between human SCOT and GCT is only 5% according to the published sequence alignment (*17*). Consequently, there are stretches of the sequences with no correspondence and for which no model was built. In contrast, the sequence identity between human SCOT and pig heart SCOT is 92%: pig heart SCOT is a very good homologue of the human enzyme. We present here the first experimentally determined structure of a CoA transferase from a mammalian source. Instrumental to the structure determination were selenomethionine substitution and the use of argon during the purification and crystallization to preclude oxidative damage.

EXPERIMENTAL PROCEDURES

Expression and Purification of Selenomethionine CoA Transferase. The expression plasmid for pig heart CoA transferase (*18*) was transformed into *E. coli* strain BL21-(DE3)pLysS to provide tight control of protein expression. To favor the production of selenomethionine protein, the biosynthesis of methionine was minimized by including high concentrations of isoleucine, lysine, and threonine in the media to inhibit the *E. coli* aspartokinases (*19*). Phenylalanine, leucine, and selenomethionine were also added to the media. Specifically, 50 μL of a glycerol stock of the

transformed *E. coli* was used to inoculate 100 mL of Luria-Bertani (LB) broth containing 0.1 μg/mL ampicillin and 0.03 μg/mL chloramphenicol. This culture was grown overnight at 37 °C, and the cells were harvested by centrifugation (5 min at $4 \times 10^3 \times g$) at room temperature. The cell pellet was resuspended in 10 mL minimal media which was used to inoculate a 2 L culture of minimal media. This culture was grown at 37 °C to an optical density at 600 nm (OD_{600}) of 0.836. The culture was moved to room temperature for the addition of the amino acids (100 mg selemethionine, 200 mg lysine−HCl, 200 mg threonine, 200 mg phenylalanine, 100 mg leucine, 100 mg isoleucine, and 100 mg valine) and then returned to 37 °C with shaking for 15 min, followed by shaking at room temperature for a further 15 min. Protein expression was induced with the addition of isopropyl-β-D-thiogalactoside (IPTG), to a final concentration of 1.0 mM. The culture was grown overnight at room temperature, to a final OD_{600} of 1.69.

Using degassed solutions, layering argon over each solution that contained the selenomethionine CoA transferase, and minimizing the time for purification and crystallization were essential for obtaining high quality crystals for the multiwavelength anomalous dispersion (MAD) experiment. Cells harvested by centrifugation (10 min, $4 \times 10^3 \times g$) were resuspended in degassed sonication buffer (0.05 M K(phosphate), 0.5 mM ethylenediaminetetraacetic acid (EDTA), 10 mM 2-mercaptoethanol, pH 7.4) and layered with argon before freezing at −70 °C. Purification of the protein was conducted at 4 °C. The frozen cell suspension was thawed and sonicated and then centrifuged to remove cell debris (30 min, $27 \times 10^3 \times g$). Solid ammonium sulfate was added to bring the concentration to 20% (w/v), the sample centrifuged (30 min, $27 \times 10^3 \times$ g), and the supernatant retained. The concentration of ammonium sulfate was increased to 50% (w/v) to precipitate the CoA transferase, the sample centrifuged (30 min, $27 \times 10^3 \times g$), and the precipitate retained. The precipitate was dissolved in approximately 5 mL degassed buffer A (5.0 mM TrisCl, 0.5 mM benzamidine, 0.2 mM EDTA, 20 mM 2-mercaptoethanol, pH 8.0), clarified by centrifugation (30 min, $27 \times 10^3 \times$ g), and desalted on a Sephadex G-25 column (2.5 × 60 cm) previously equilibrated with buffer A. The resultant sample was then loaded on a DEAE-Sephacel column (5.0 × 10 cm) and eluted with a continuous gradient of buffer A containing 0−0.5 M KCl. Fractions containing active enzyme were pooled and concentrated using a Centriprep 50 k molecular weight cutoff membrane. This concentrated pool, containing approximately 0.125 M KCl in buffer A was loaded directly on a Blue Sepharose 6 Fast Flow column (2.5 × 20 cm) previously equilibrated with buffer A. The selenomethionine CoA transferase was eluted with a continuous gradient of buffer A containing 0−2.0 M KCl. Fractions containing the active enzyme (between 0.125 and 0.5 M KCl) were pooled and concentrated to 22.8 mg/mL. The final yield of purified selenomethionine CoA transferase was 6.8 mg, and the concentrated protein solution was stored under argon at 4 °C until set up for crystallization.

Structure Determination of Selenomethionine CoA Transferase. Crystals were grown by the hanging drop method. The well solution contained 20% (w/v) poly(ethylene glycol) 2000 (P2000) dissolved in 100 mM TrisCl, pH 8.0. Small droplets (0.9 μL) mixing 0.4 μL of the protein solution and 0.5 μL of the well solution were suspended on the plastic cover slips. Crystallization trays were set up quickly in large plastic bags filled with argon in order to minimize oxidation of the selenomethionine residues. The trays were incubated at 21 °C, and crystals grew in 1−2 days. For collection of the diffraction data, large, single crystals were soaked for a short time (<10 s) in a cryosolution of 20% (w/v) P2000, 100 mM TrisCl, pH 8.0, and 20% (v/v) glycerol before being vitrified in a nitrogen stream at 100 K and exposed to X-rays. After preliminary screening, the best diffracting crystals were stored in a cryodewar and shipped to Brookaven National Laboratory for MAD data collection on beamline X26c. The peak, inflection, and remote wavelengths of 0.978, 0.979, and 0.961 Å were chosen according to the fluorescence scan. Diffraction intensities were measured with an Area Detector Systems Quantum 4 CCD detector (*20*) set at a crystal to detector distance of 250 mm, and the data were processed with the program HKL2000 (*21*). "Shake-and-Bake" (*22*, *23*), as implemented in the computer program SnB v2.1 (*24*), was used to find the initial sites of the anomalously scattering atoms with the data set collected at the wavelength of the inflection point. SnB searched for 52 atoms, since there are 13 methionine residues in one molecule, and four molecules expected in the asymmetric unit of the $P2_1$ cell. Coordinates for the highest 26 peaks were then put into the computer program SOLVE/RESOLVE to search for the remaining 26 sites, to refine their positions, to calculate and modify the electron density using solvent flattening and noncrystallographic symmetry and to build in the protein backbone atoms (*25*−*32*). Using the coordinates for the backbone atoms from RESOLVE and electron density maps calculated with programs from the CCP4 Package (*33*) using Hendrickson−Lattman coefficients, a model for one of the four molecules in the asymmetric unit was built using the interactive graphics program XFIT (*34*). This model was rotated and translated to fit into the electron density for the other three monomers. Rigid body refinement was done with the computer program Crystallography and NMR System (CNS) (*35*), initially treating the four monomers as separate units, followed by splitting the monomers into their amino- (1−250) and carboxy-terminal (260−481) domains for another round of rigid body refinement. Refinement by simmulated annealing and energy minimization were next performed with CNS, using the noncrystallographic symmetry as a restraint. More atoms were added to the model and 13 cycles of building and refinement ensued. The NCS restraints were removed only for the residues whose conformations were different in the four monomers. The computer program PROCHECK was used to evaluate the geometry (*36*).

RESULTS

Prior to the extensive use of argon during purification protocols and crystallization setups, our attempts to solve the structure of pig heart CoA transferase using the MAD signal from the selenium atoms were unsuccessful because of the poor quality of the crystals. The initial crystals were small, tended to "rubberize" losing their ability to diffract X-rays, and had problems with high mosaicity. The high mosaicity made data collection difficult because the unit cell has one long edge of approximately 264 Å. Perhaps because of their small size, these crystals decayed during the MAD data collection.

Table 1: Statistics for Crystallographic Data

data set	peak	inflection	remote
wavelength (Å)	0.978	0.979	0.961
cell dimensions	$a = 60.17$ Å	$a = 60.14$ Å	$a = 60.12$ Å
	$b = 264.3$ Å	$b = 264.3$ Å	$b = 264.2$ Å
	$c = 62.69$ Å	$c = 62.66$ Å	$c = 62.64$ Å
	$\alpha = \gamma = 90°$	$\alpha = \gamma = 90°$	$\alpha = \gamma = 90°$
	$\beta = 111.88°$	$\beta = 111.87°$	$\beta = 111.86°$
resolution range (Å)	30−2.5	30−2.5	30−2.5
number of measurements	414407	417593	419275
number of unique reflections	61401	61118	61460
R_{merge}[a]	0.085	0.069	0.069
R_{merge} in high-resolution shell	0.188	0.149	0.150
(resolution range, Å)	(2.59−2.50)	(2.59−2.50)	(2.59−2.50)
$\langle I\rangle/\langle\sigma(I)\rangle$[b]	27.42	30.25	29.76
$\langle I\rangle/\langle\sigma(I)\rangle$ in high-resolution shell	6.99	7.99	8.25
(resolution range, Å)	(2.59−2.50)	(2.59−2.50)	(2.59−2.50)
completeness (%)	97.9	97.9	98.8
completeness in high-resolution shell (%)	84.3	85.7	90.5
(resolution range, Å)	(2.59−2.50)	(2.59−2.50)	(2.59−2.50)

[a] $R_{merge} = (\sum\sum|I_i - \langle I\rangle|)/\sum\sum\langle I\rangle$, where I_i is the intensity of an individual measurement of a reflection and $\langle I\rangle$ is the mean value for all equivalent measurements of this reflection. [b] $\langle I\rangle$ is the mean intensity for all reflections, and $\langle\sigma(I)\rangle$ is the mean sigma for these reflections.

When very careful attention was paid toward the prevention of oxidation and proteolysis, much better crystals were obtained. After the crystallization trays were set up in an atmosphere of argon, these crystals appeared quickly, often within minutes, and grew to sizes of approximately 0.1 mm × 0.1 mm × 0.3 mm in 1−2 days. The selenomethionine pig heart SCOT crystallized in space group $P2_1$, with four molecules in the asymmetric unit. A complete MAD data set could be collected from a single crystal in the resolution range of 30−2.5 Å. Statistics from the data collection and processing steps can be found in Table 1.

SnB successfully found the initial selenium substructure from the anomalous differences present in the inflection data set. The computer program SOLVE/RESOLVE was then able to find additional peaks and calculate a selenium-phased, solvent-flattened electron density map with a figure of merit of 0.699. Figure 1A shows part of this map near the amino-terminus of monomer D. Elements of secondary structure were apparent in the map as were the locations of the selenomethionine residues. Model building and refinement resulted in a model that included residues 1−250 and 260−481 for monomers A and D and residues 1−250 and 259−481 for monomers B and C. Positional coordinates and tightly restrained *B*-factors were refined for each atom. The refinement statistics are listed in Table 2. A portion of the final electron density map is illustrated in Figure 1B. Final coordinates as well as data have been deposited in the Protein Data Bank (*37*) where they have been assigned PDB identifier 1M3E and RCSB identifier RCSB016547.

DISCUSSION

Pig heart SCOT is an α/β protein (Figure 2). The overall fold of the monomer polypeptide chain is similar to that of the GCT heterodimer (Figure 3). The similarity between the two structures extends to the quaternary structure: the homodimer formed by pig heart SCOT monomers in our crystal structure (Figure 2, panels A (blue) and B (green) or C (yellow) and D (violet)) is similar to the heterotetramer formed by the dimerization of two GCT heterodimers. The amino-terminal portion of SCOT superposes onto subunit A of the bacterial enzyme and the carboxy-terminal portion, containing the active site glutamate residue, Glu 305, superimposes onto subunit B. A sequence alignment based on the structural superpositions is shown in Figure 4. In total, there are 73 identical residues in this alignment, 44 from the amino-terminal portion of SCOT and 29 from the carboxy-terminal portion. Since there are 481 amino acid residues in SCOT, the sequence identity is 15%. This value is considerably higher than the 5% that had been predicted from the sequences even when the structure of GCT was known. Even this number is lower than the similarity usually needed to solve a structure by molecular replacement methods.

The longest stretch for which there is no superposition runs from residue 125 to residue 157 in SCOT and A129 to A164 in GCT. In SCOT these residues form a short helix, followed by three β-strands that fold into a twisted β-hairpin. This β-hairpin extends the β-sheet in SCOT. The second longest stretch that does not superpose is the linker region of SCOT, for which there is no equivalent in GCT. The two domains of pig heart SCOT are linked by this "hinge" region which is known to be readily nicked by proteases between residues Gly 256 and Lys 257 (*10*). Residues from the hinge region, 251−259 (251−258 in monomers B and C), are not visible in the electron density maps. This could be due to nicking of the enzyme; however, residues 250 and 260 are close enough in space (16 Å) to be joined by the nine intervening amino acid residues, and the electron density for these intervening residues may not be visible simply because the residues adopt multiple conformations.

A tetrameric form of SCOT has been observed in enzyme that has been partially purified from pig heart tissue, as well as in enzyme overexpressed in *E. coli* (*14*). Although four monomers make up the asymmetric unit in our crystals (Figure 2), it seems unlikely that the interface observed between the two homodimers, i.e., between monomers B (green) and C (yellow), is that of the physiologically relevant tetramer. This interpretation is based on close examination of the interface. While the surface area buried between monomers A and B is 3849 Å^2 and the buried surface area between the amino- and carboxy-terminal domains is 3517 Å^2, that buried between monomers B and C is only 1871

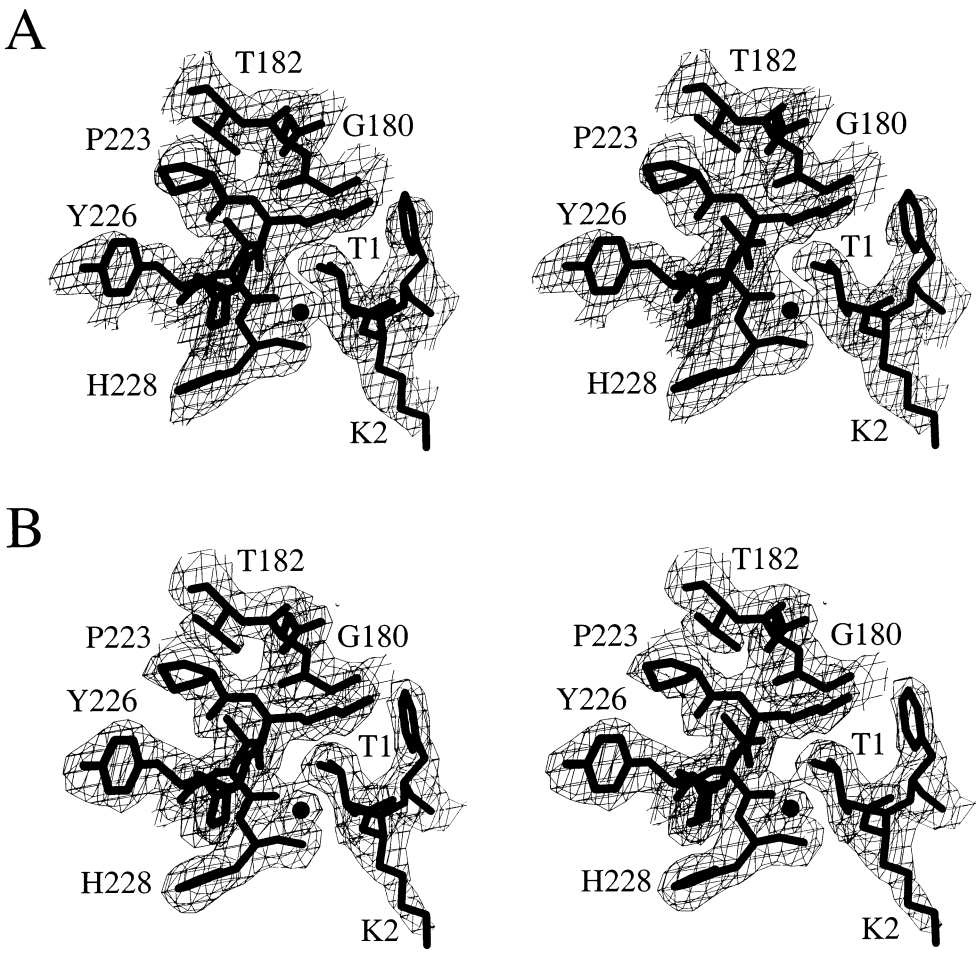

FIGURE 1: Electron density at the amino terminus of monomer D. The electron density is from $2F_o-F_c$ maps, contoured at 1σ. The model is drawn in thick lines, while the map is drawn in thin lines. (A) The initial electron density map is shown superimposed on the final refined model. (B) The final electron density map is shown with the final model. This figure was drawn using the programs BOBSCRIPT and MOLSCRIPT (*39*, *40*).

Table 2: Refinement Statistics for the Final Model

R-factor[a]	22.1%
R^b_{free}(5% of data)	26.5%
number of protein atoms	14441
number of water molecules	859
rms deviations from ideal geometry	
bond lengths	0.006 Å
bond angles	1.4°
Ramachandran plot statistics for nonproline and nonglycine residues	
number in most favored regions	1428 (88.5%)
number in additional allowed regions	163 (10.1%)
number in generously allowed regions	17 (1.0%)
number in disallowed regions	6 (0.4%)

[a] $R = \sum||F_o| - |F_c||/\sum|F_o|$. [b] R-factor based on data excluded from the refinement.

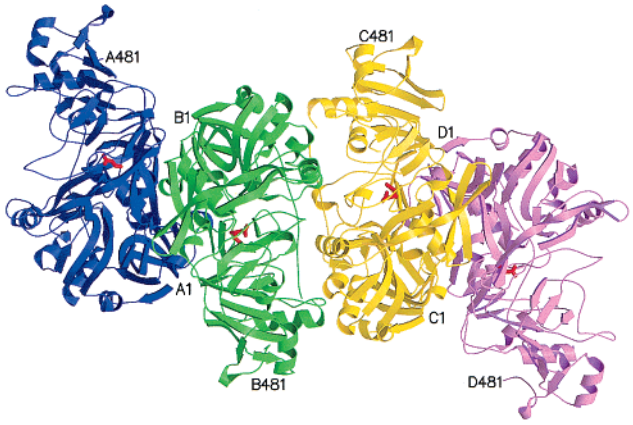

FIGURE 2: Ribbon diagram of the four SCOT monomers in the asymmetric unit. The amino- and carboxy-terminal residues of each monomer are labeled. The side chain of the active site residue, Glu 305, has been depicted as a red stick model in each monomer. The physiological dimers are formed by monomers A (blue) and B (green) and monomers C (yellow) and D (violet). This figure as well as Figures 3 and 5 were drawn using the programs MOLSCRIPT and RASTER3D (*40*−*42*).

Å^2. While the amino- and carboxy-terminal domains as well as the monomers A and B associate with each other via hydrophobic interactions and a few short β-sheet hydrogen-bonding interactions, the interactions at the surface between monomers B and C are nonspecific, often bridged by water molecules. The temperature factors of residues at the interfaces are also quite different. At the intramonomer and intradimer interfaces, the temperature factors are similar to those in the interior of the protein, while those at the interface between monomers B and C are higher, like those on the protein's surface. The higher temperature factors indicate the greater flexibility of the residues at this interface. The protocol for the purification of the selenomethionine protein leaves the protein in a relatively high concentration of potassium chloride, and therefore the physiological tetrameric form would not be expected, but the dimer would be favored.

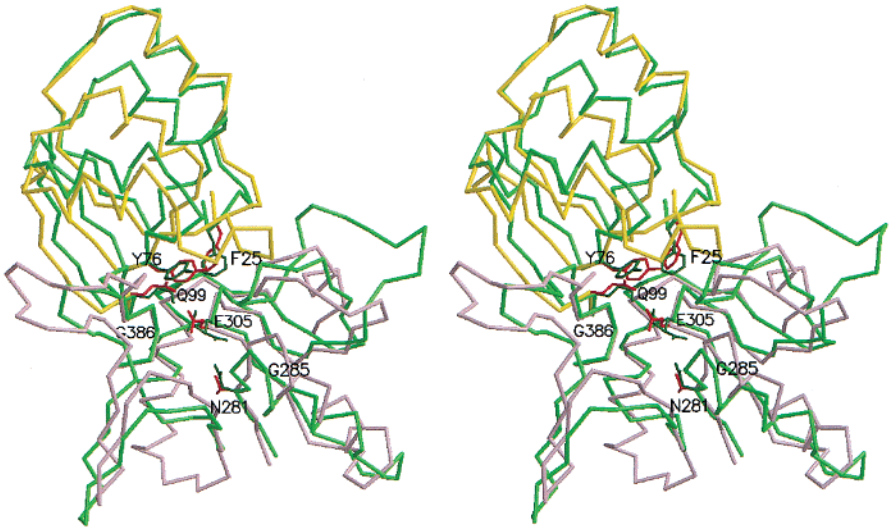

FIGURE 3: Superposition of the Cα traces of GCT and SCOT. For GCT, only residues A25-A104 and B25−B139 shown in yellow and pink, respectively, are depicted. For SCOT, only residues A24-A100 and A278-A388 shown in green are depicted. Side-chain atoms from selected residues of SCOT have been drawn as dark green sticks and are labeled, while those from the equivalent residues of GCT have been drawn as red sticks.

Four of the six residues in the disfavored regions of the Ramachandran plot have clear electron density, so we are confident of their conformations. The four are Asn 190 in the four chains. This residue is in the second position of a β-turn, where the carbonyl oxygen atom of residue Arg 189 accepts a hydrogen-bond from the amide nitrogen atom of residue Asn 192. The disfavored conformation of Asn 190 is also stabilized by hydrogen bonds with its main- and side-chain atoms: between its amide nitrogen atom and a buried water molecule (visible in all chains except D); between its carbonyl oxygen atom and the amide nitrogen atom of residue Ser 343; between Nδ2 and the carbonyl oxygen atoms of residues Ser 187 and Ala 188; and between Oδ1 and the amide nitrogen atoms of residues Gly 24 and Phe 191. The other two residues with disfavored backbone conformations, residues selenomethionine 384 and Ala 394 of chain D, are in regions with poor electron density and we are less confident of their conformations. The electron density is likely to be that from multiple conformations of the residues, to which we have fitted a single conformation for the residues.

A close examination of the active sites from the mammalian and bacterial enzymes (Figures 3 and 5) is very informative. The residues Gly 385, Gly 386, and Ala 387 that form part of the predicted oxyanion hole (*16*) superpose very well with the equivalent residues in GCT (Figure 3). On the basis of the structure of GCT, Jacob et al. hypothesized that the amide groups of the GCT residues that are equivalent to Gln 99 and Gly 386 would stabilize the negative charge on the side chain of the active site glutamate residue in the tetrahedral transition state (*16*). Main-chain atoms from several other conserved residues also superpose, including Phe 25, Tyr 76, Gln 99, and the catalytic Glu 305. However, although the side chains for Phe 25, Tyr 76, and Gln 99 point in similar directions as the corresponding side chains in GCT, they do not superpose. Surprisingly, the side-chain atoms for Glu 305 do not adopt a single conformation among the four monomers in the asymmetric unit of the crystals of SCOT (Figure 5). In monomers A and D, Glu 305 adopts one conformation, with hydrogen-bonding interactions to water molecules in the active site. Two alternate conformations are apparent from the electron density for Glu 305 in monomers B and C. In the first conformation, Glu 305 forms hydrogen bonds with Gln 99 and a water molecule; and in the alternate conformation, it forms hydrogen bonds with Asn 281 and a water molecule. This flexibility may be integral to the catalytic mechanism with the glutamate side chain adopting one conformation when substrate is noncovalently bound and another when the covalent bond is being formed. We wonder if this reflects the idea that only one subunit supports catalysis (*15*). It will be interesting to learn what conformation the active site glutamate residue adopts in complexes with substrates or substrate analogues.

Near the active site glutamate residue, there are differences between SCOT and GCT in the conformations of several loops. The most obvious difference is that the loop between residues 74 and 82 in SCOT is longer in GCT by six residues, supporting the interpretation by Jacob et al. that this loop plays a role in binding glutaconate specifically (*16*). A second loop in SCOT includes residues Glu 241 and Arg 242, which occupy, along with Lys 329, the space of the longer loop in GCT. The three charged residues may play a role in the binding of succinate or acetoacetate.

Two of the several missense mutations in human SCOT that were reported by Fukao et al. for patients suffering ketoacidosis are Val 182 to Met and Gly 180 to Glu (*17*). According to their homology model constructed for human SCOT based on the GCT structure, Fukao et al. suggested that these mutations might disrupt dimer formation in the mammalian enzyme. Indeed, these residues are located near the dimer interface, but we further propose that these mutations would disrupt folding of the amino-terminal domain. Gly 180 adopts a conformation that would be disfavored for residues that have side chain atoms. As well, it is within van der Waals contact distance of Oγ1 of the amino-terminal threonine residue, which donates a hydrogen bond to the carbonyl oxygen atom of Val 227. The equivalent glycine residue in GCT is similarly close to the hydrogen bond formed between Nζ of Lys 3 and the carbonyl oxygen atom of Val 236 O (GCT numbering). From this evidence,

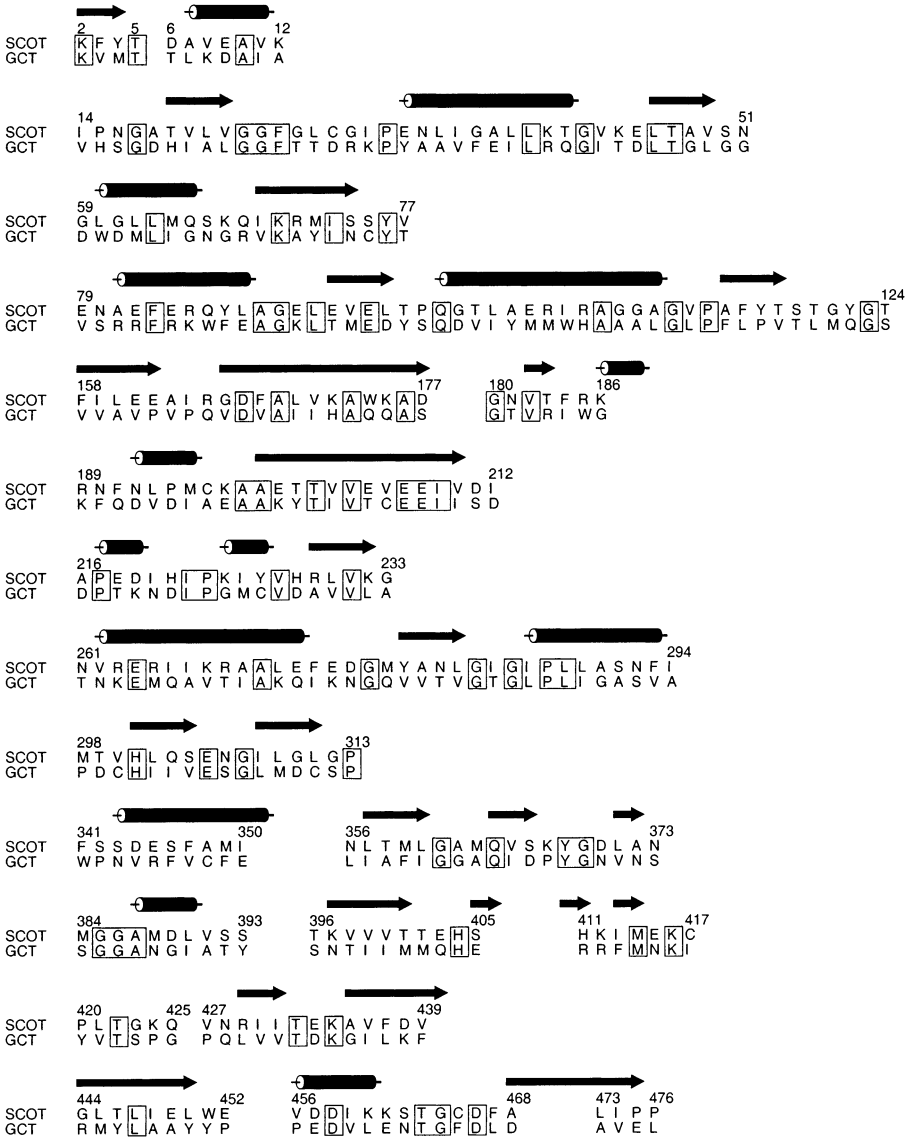

FIGURE 4: Sequence alignment of SCOT with GCT, based on the two structures. The models were superposed using the program O (*43*). First, the amino-terminal residues of SCOT were superposed with GCT; then the superposition was repeated for the carboxy-terminal residues. Only residues that superposed within 2.8 Å are shown in the alignment. When the residues of SCOT are found in α-helices or *β*-strands, these elements of secondary structure are depicted above the sequence alignment. The numbering given corresponds to SCOT. This figure was drawn using the program ALSCRIPT (*44*).

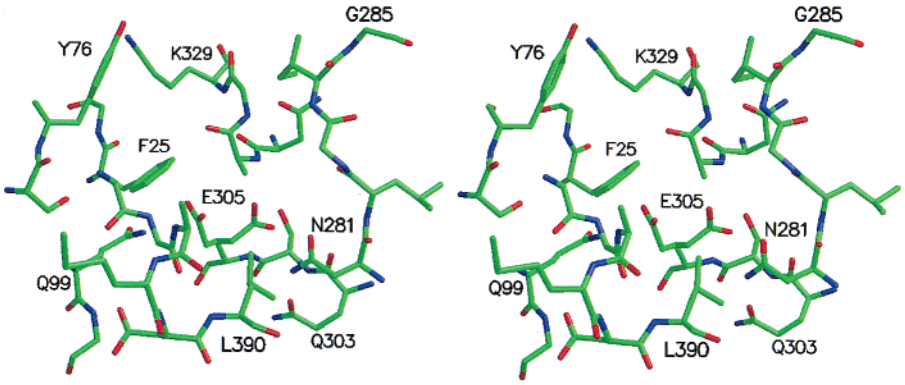

FIGURE 5: Close-up view in stereo of the active site. The model is colored according to atom type: oxygen atoms are red, nitrogen atoms are blue, and carbon and selenium atoms are green. Both of the conformations for the side chain of active site residue Glu 305 have been included in the figure.

we suggest that a mutation of Gly 180 to Glu would disrupt the stabilization of the amino-terminal strand, possibly interfering with the proper folding of the amino-terminal domain. It is more difficult to predict the detrimental effect that the Val 182 to Met missense mutation might have on domain folding. Perhaps the *β*-branched valine residue at

this position restricts conformation of the main chain more than a methionine residue would. This extra inflexibility might discourage the efficient folding of the amino-terminal domain.

This first determination of the structure of a mammalian CoA transferase serves as a reminder of the limitations of a homology model, emphasizing the limitation of extrapolation from a prokaryotic structure to mammalian systems. For the determination of the structure of pig heart SCOT, two experimental improvements were essential: increasing the speed of purification, to limit proteolytic cleavage and oxidation; and protecting the protein sample from oxidation using argon. On the basis of the detailed model of the structure now available, site-directed mutagenesis experiments can be designed to further investigate the catalytic mechanism and to gain an understanding of how different CoA transferases interact with their various substrates/products.

ACKNOWLEDGMENT

We thank Howard Robinson, Annie Heroux, and Randall McNally at NSLS for collecting the MAD diffraction data. We thank Ziya Dhalla, Rachel Burdett, Chris Rochet, Kenneth Ng, and Craig Garen for their technical assistance and suggestions.

REFERENCES

1. Niezen-Koning, K. E., Wanders, R. J. A., Ruiter, J. P. N., Ijlst, L., Visser, G., Reitsma-Bierens, W. C. C., Heymans, H. S. A., Reijngoud, D. J., and Smit, G. P. A. (1997) *Eur. J. Pediatr. 156*, 870−873.
2. Snyderman, S. E., Sansaricq, C., and Middleton, B. (1998) *Pediatrics 101*, 709−711.
3. Hersh, L. B., and Jencks, W. P. (1967) *J. Biol. Chem. 242*, 3468−3480.
4. Edwards, M. R., Singh, M., and Tubbs, P. K. (1973) *FEBS Lett. 37*, 155−158.
5. White, H., and Jencks, W. P. (1976) *J. Biol. Chem. 251*, 1708−1711.
6. Sharp, J. A., and Edwards, M. R. (1978) *Biochem. J. 173*, 759−765.
7. Russell, J. J., and Patel, M. S. (1982) *J. Neurochem. 38*, 1446−1452.
8. Solomon, F., and Jencks, W. P. (1969) *J. Biol. Chem. 244*, 1079−1081.
9. Moore, S. A., and Jencks, W. P. (1982) *J. Biol. Chem. 257*, 10893−10907.
10. Lin, T. W., and Bridger, W. A. (1992) *J. Biol. Chem. 267*, 975−978.
11. Rochet, J. C., and Bridger, W. A. (1994) *Prot. Sci. 3*, 975−981.
12. Howard, J. B., Zieske, L., Clarkson, J., and Rathe, L. (1986) *J. Biol. Chem. 261*, 60−65.
13. Williams, W. A. (1990) University of Minnesota.
14. Rochet, J. C., Brownie, E. R., Oikawa, K., Hicks, L. D., Fraser, M. E., James, M. N. G., Kay, C. M., Bridger, W. A., and Wolodko, W. T. (2000) *Biochemistry 39*, 11291−11302.
15. Lloyd, A. J., and Shoolingin-Jordan, P. M. (2001) *Biochemistry 40*, 2455−2467.
16. Jacob, U., Mack, M., Clausen, T., Huber, R., Buckel, W., and Messerschmidt, A. (1997) *Structure 5*, 415−426.
17. Fukao, T., Mitchell, G. A., Song, X.-Q., Nakamura, H., Kassovska-Bratinova, S., Orii, K. E., Wraith, J. E., Besley, G., Wanders, R. J. A., Niezen-Koning, K. E., Berry, G. T., Palmieri, M., and Kondo, N. (2000) *Genomics 68*, 144−151.
18. Rochet, J.-C., Oikawa, K., Hicks, L. D., Kay, C. M., Bridger, W. A., and Wolodko, W. T. (1997) *Biochemistry 36*, 8807−8820.
19. Doublie, S. (1997) in *Methods in Enzymology* (Carter, C. W. J., and Sweet, R. M., Eds.) pp 523−530.
20. Szebenyi, D. M. E., Arvai, A., Ealick, S., LaIuppa, J. M., and Nielsen, C. (1997) *J. Synchrotron Rad. 4*, 128−135.
21. Otwinowski, Z., and Minor, W. (1997) in *Methods in Enzymology* (Carter, C. W., and J. R. M. S., Eds.) pp 307−326, Academic Press, New York.
22. Weeks, C. M., DeTitta, G. T., Miller, R., and Hauptman, H. A. (1993) *Acta Crystallogr. D49*, 179−181.
23. Weeks, C. M., DeTitta, G. T., Hauptman, H. A., Thuman, P., and Miller, R. (1994) *Acta Crystallogr. A50*, 210−220.
24. Weeks, C. M., and Miller, R. (1999) *J. Appl. Crystallogr. 32*, 120−124.
25. www.solve.lanl.gov..
26. Terwilliger, T. C., and Eisenberg, D. (1983) *Acta Crystallogr. A43*, 6−13.
27. Terwilliger, T. C., Kim, S.-H., and Eisenberg, D. (1987) *Acta Crystallogr. A43*, 1−5.
28. Terwilliger, T. C., and Eisenberg, D. (1987) *Acta Crystallogr. A43*, 6−13.
29. Terwilliger, T. C. (1994) *Acta Crystallogr. D50*, 11−16.
30. Terwilliger, T. C. (1994) *Acta Crystallogr. D50*, 17−23.
31. Terwilliger, T. C., and Berendzen, J. (1997) *Acta Crystallogr. D53*, 571−579.
32. Terwilliger, T. C., and Berendzen, J. (1999) *Acta Crystallogr. D55*, 849−861.
33. Collaborative Computational Project, No. 4 (1994) *Acta Crystallogr. D50*, 760−763.
34. McRee, D. E. (1999) *J. Struct. Biol. 125*, 156−165.
35. Brunger, A. T., Adams, P. D., Clore, G. M., Delano, W. L., Gros, P., Grosse-Kunstleve, R. W., Jiang, J.-S., Kuszewski, J., Jilges, N., Pannu, N. S., Read, R. J., Rice, L. M., Simonson, T., and Warren, G. L. (1998) *Acta Crystallogr. D54*, 905−921.
36. Laskowski, R. A., MacArthur, M. W., Moss, D. S., and Thornton, J. M. (1993) *J. Appl. Crystallogr. 26*, 283−291.
37. Berman, H. M., Westbrook, J., Feng, Z., Gilliland, G., Bhat, T. N., Weissig, H., Shindyalov, I. N., and Bourne, P. E. (2000) *Nucleic Acids Res. 28*, 235−242.
38. Selmer, T., and Buckel, W. (1999) *J. Biol. Chem. 274*, 20772−20778.
39. Esnouf, R. M. (1997) *J. Mol. Graphics 15*, 132−134.
40. Kraulis, P. J. (1991) *J. Appl. Crystallogr. 24*, 946−950.
41. Bacon, D. J., and Anderson, W. F. (1988) *J. Mol. Graphics 6*, 219−220.
42. Merritt, E. A., and Bacon, D. J. (1997) in *Methods in Enzymology* (Carter, C. W., and J. R. M. S., Eds.) pp 505−524, Academic Press, New York.
43. Jones, T. A., Zou, J. Y., Cowan, S. W., and Kjeldgaard, M. (1991) *Acta Crystallogr. A47*, 110−119.
44. Barton, G. J. (1993) *Protein Eng. 6*, 37−40.

BI020568F